Experimental Mechanics (2009) 49:439–450
DOI 10.1007/s11340-008-9167-8

Time Average Geometric Moiré—Back to the Basics

M. Ragulskis · Z. Navickas

Received: 11 October 2007 / Accepted: 30 June 2008 / Published online: 2 August 2008

Abstract Applicability of time average geometric moiré for elastic oscillating structures is analysed in this paper. Mathematical and numerical models describing the formation of time averaged fringes are carefully constructed without the assumption that dynamic deflections are described by a slowly varying function. Though time average geometric moiré is considered as a classical optical experimental technique, we show that well known relationship between the fringe order, amplitude of oscillation and pitch of the grating in state of equilibrium can be used only when the amplitude is small. Otherwise the inverse problem of fringe interpretation becomes much more complicated and is the object of analysis in this paper. We describe the interpretation of fringes produced by time average geometric moiré in detail and illustrate the complexity of the problem by numerical examples.

Keywords Time average moiré · Bessel functions · Inverse problem · Pattern of fringes · Convergence

Introduction

Advanced strain measurement and control tools (including geometric moiré techniques) are regarded as primary technology drivers in such industries as MEMS (micro-electro-mechanical systems) fabrication and high precision machine tools manufacturing [1–4]. Accurate interpretation of measurement results is one of the crucial factors enabling minimization of errors and uncertainties in the manufacturing process.

Geometric moiré [4, 5] is a classical in-plane whole field non-destructive optical experimental technique based on analysis of visual patterns produced by superposition of two regular gratings that geometrically interfere. Examples of gratings are equispaced parallel lines, concentric circles, arrays of dots, etc. [5, 6]. The gratings can be superposed by double-exposure photography, by reflection, by shadowing, or by direct contact [7, 8]. Moiré patterns are used to measure variables such as displacements, rotations, curvature, and strain throughout the viewed area. In-plane moiré is typically conducted with gratings of equispaced, parallel lines painted on the surface of the analyzed body [5, 7].

Double-exposure geometric moiré techniques can be extended to time-average geometric moiré methods when the moiré grating is formed on the surface of elastic oscillating structure and time averaging techniques are used for registration of time averaged patterns of fringes [9, 10]. These seminal papers exploit assumptions that dynamic in-plane displacements from the state of equilibrium can be different at different locations on the measured surface. Nevertheless, the mathematical relationships in these papers declare that the pitch of moiré grating is assumed to be almost constant even in the state of maximum deformations. Elegant mathematical transformations are used to derive a relationship between the order of time averaged fringe, pitch of the grating in the state of equilibrium and the magnitude of dynamic displacement. It is shown that time averaged fringe order no longer represents the displacement by an integer number of pitches; the intensity of time averaged moiré pattern is governed by mathematical

M. Ragulskis (✉, SEM Member) · Z. Navickas
Department of Fundamental Sciences,
Kaunas University of Technology,
Studentu 50-222,
Kaunas 51638, Lithuania
e-mail: minvydas.ragulskis@ktu.lt

Z. Navickas
e-mail: zenonas.navickas@ktu.lt

relationships comprising more complex mathematical relationships involving Bessel functions of the first kind.

These classical results are represented in textbooks on experimental mechanics [4] and are exploited in numerous engineering applications involving time average projection, reflection, and geometric moiré [11–13]. But it appears that mathematical relationships governing the formation of time averaged fringes become much more complex than reported by Dai and Wang [8] and Liang et al. [9] if the variation of the pitch of the moiré grating in time is assumed without any simplifications.

The goal of this paper is to follow the derivation of these mathematical relationships as strictly as possible so as to enable deeper understanding of the physical information represented by fringes produced by time average geometric moiré.

One-dimensional Example, Basic Formulations

One-dimensional example is analyzed for simplicity at first. Moiré grating on the surface of a one-dimensional structure in the state of equilibrium can be interpreted as a periodic variation of black and white colors. Continuous harmonic moiré functions are well applicable for digital image processing in computational environments [5, 13]:

$$M_1(x) = \frac{1}{2}\left(1 + \cos\left(\frac{2\pi}{\lambda}x\right)\right) = \cos^2\left(\frac{\pi}{\lambda}x\right) \tag{2.1}$$

where x is the longitudinal coordinate; M_1 is grayscale intensity of the surface at point x; λ is the pitch of the grating. Numerical value of 0 of the function in equation (2.1) corresponds to black color; 1 corresponds to white color and all intermediate values correspond to appropriate grayscale levels.

The grating of one-dimensional structure in a deformed state can be interpreted as follows

$$M_2(x + u(x)) = M_1(x) = \cos^2\left(\frac{\pi}{\lambda}x\right) \tag{2.2}$$

where $u(x)$ is in-plane deformation at point x. Clearly, equation (2.2) is implicit. It would be tempting to express M_2 in an explicit form using transformation $M_2(x) = \cos^2\left(\frac{\pi}{\lambda}(x - u(x))\right)$, but this would lead to a crude mathematical mistake (we will illustrate this error in Fig. 1).

Unfortunately the only possible way to produce an explicit form of equation (2.2) is to solve the following relationship (to express x as a function of z):

$$x + u(x) = z \tag{2.3}$$

which generally may not have a unique solution. If this equation (2.3) can be solved, and the solution can be expressed in the form $x = v(z)$, then M_2 can be expressed in the explicit form:

$$M_2(x) = M_1(v(x)) = \cos^2\left(\frac{\pi}{\lambda}v(x)\right). \tag{2.4}$$

But it is a quite common practice to describe the deformed grating using incorrect explicit relationship:

$$M_3(x) = M_1(x - u(x)) = \cos^2\left(\frac{\pi}{\lambda}(x - u(x))\right). \tag{2.5}$$

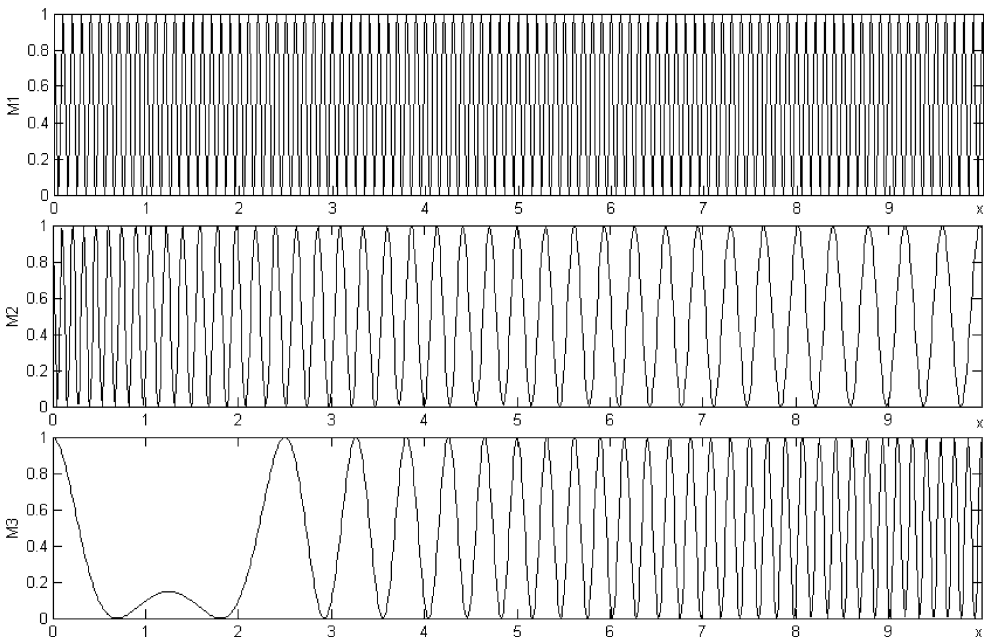

Fig. 1 One-dimensional gratings $M_1(x)$, $M_2(x)$ and $M_3(x)$ at $u(x)=kx^2$ and $\lambda=0.1$; $k=0.4$

A few examples can illustrate this tendency: [10] (eq. (4), page 64); [5] (eq. (1.1), page 2); [14] (eq. (6), page 3); [15] (eq. (2), page 297). In fact, the expression in equation (2.5) is correct only when the field of deformation $u(x)$ does not depend on x (solid non-deformable body is deflected from the state of equilibrium without being deformed). Then $u(x)=u$; $x=z-u$, and $M_2(x)=M_1(x-u)$. But this is not true in the general case.

In order to illustrate this fact we assume that the one-dimensional field of deformations is defined as $u(x)=kx^2$, where k is a constant. Clearly, the pitch of the deformed grating should increase as x increases. Equation $x+kx^2=z$ produces $x=\left(-1+\sqrt{1+4kz}\right)/2k$. Thus, $M_2(x)=\cos^2\left(\frac{\pi\left(-1+\sqrt{1+4kx}\right)}{2\lambda k}\right)$. Numerically reconstructed one-dimensional gratings are presented in Fig. 1 and clearly illustrate the incorrectness of formulation in equation (2.5). It must be noted that the values of functions M_1, M_2 and M_3 in Fig. 1 correspond not to the height of the surface but to the grayscale levels of the surface which remains flat also in the deformed state.

Particularly, when the deformation is a linear function $u(x)=kx$, the deformed grating is $M_2(x)=\cos^2\left(\frac{\pi}{\lambda(1+k)}x\right)$, not $M_3(x)=\cos^2\left(\frac{\pi(1-k)}{\lambda}x\right)$. Function M_2 has a singular point at $k=-1$. That is quite natural—one dimensional structure is compressed into a single point at coordinate $x=0$. The pitch of the deformed grating is $\lambda(1+k)$. When $k=1$ the pitch of the deformed grating becomes 2λ. But function $M_3(x)=1$ at $k=1$. That is a consequence of incorrect mathematical formulation of the problem.

Additive superposition [5] of the original and the deformed gratings yields:

$$\begin{aligned}&\tfrac{1}{2}\left(\cos^2\left(\tfrac{\pi}{\lambda}x\right)+\cos^2\left(\tfrac{\pi}{\lambda(1+k)}x\right)\right)\\&=\tfrac{1}{2}+\tfrac{1}{2}\cos\left(\left(\tfrac{\pi}{\lambda}-\tfrac{\pi}{\lambda(1+k)}\right)x\right)\cdot\cos\left(\left(\tfrac{\pi}{\lambda}+\tfrac{\pi}{\lambda(1+k)}\right)x\right)\\&=\tfrac{1}{2}+\tfrac{1}{2}\cos\left(\tfrac{\pi k}{(1+k)\lambda}x\right)\cdot\cos\left(\tfrac{(2+k)\pi}{(1+k)\lambda}x\right)\end{aligned}\tag{2.6}$$

and the well-known effect of beats is observed. The envelope function of the beats is

$$E(x)=\frac{1}{2}\pm\frac{1}{2}\cos\left(\frac{\pi k}{(1+k)\lambda}x\right).\tag{2.7}$$

Thus the centers of moiré fringes will be located at:

$$\frac{k}{1+k}x=\lambda\left(\frac{1}{2}+n\right),\tag{2.8}$$

where $n\in\mathbf{Z}$. When k is small, $\frac{k}{1+k}x\approx kx=u(x)$, and each new moiré fringe indicates an increase or decrease of specimen deformation by one grating pitch in the direction perpendicular to the reference grating lines [4].

The requirement that the deformation must be a "slowly varying function" is raised in [5] (page 2) not without a purpose. Mathematically it means only one thing, that k is small. Otherwise the interpretation of moiré fringes becomes much more complicated. Similar simplifications can be found in other publications [16] (eq. (20), page 157); [17] (eq. (1), page 254); [18] (eq. (1), page 350). Incorrect manipulations with shifted arguments (in style of M_3) prevent derivation of the exact relationship between the fringe order and the magnitude of deformation at that point, which is even more complex when $u(x)$ is a nonlinear function.

Time Average Geometric Moiré

Similar observations can be made for time average moiré. If a solid non-deformable body oscillates around the state of equilibrium without being deformed, then the deflection from state of equilibrium does not depend on x:

$$u(x,t)=u(t)=a\sin(\omega t+\varphi),\tag{3.1}$$

where ω is the cyclic frequency, ϕ is the phase and a is the amplitude of oscillation. In that case the relationship in equation (2.3) yields: $x+a\sin(\omega t+\varphi)=z$. Thus, $x=z-a\sin(\omega t+\varphi)$, and time averaged grayscale intensity can be expressed like [9, 13]:

$$\begin{aligned}M_4(x)&=\lim_{T\to\infty}\frac{1}{T}\int_0^T\cos^2\left(\frac{\pi}{\lambda}(x-a\sin(\omega t+\varphi))\right)dt\\&=\frac{1}{2}+\frac{1}{2}\cos\left(\frac{2\pi}{\lambda}x\right)\lim_{T\to\infty}\frac{1}{T}\int_0^T\exp\left(i\frac{2\pi}{\lambda}a\sin t\right)dt\\&=\frac{1}{2}+\frac{1}{2}\cos\left(\frac{2\pi}{\lambda}x\right)J_0\left(\frac{2\pi}{\lambda}a\right)\end{aligned}\tag{3.2}$$

where i is the imaginary unit; J_0 is the 0^{th} order Bessel function of the first kind.

Then, the envelope function modulating the original grating is

$$E(a)=\frac{1}{2}\pm\frac{1}{2}J_0\left(\frac{2\pi}{\lambda}a\right).\tag{3.3}$$

The effect of formation of time averaged fringes at increasing amplitude a is illustrated in Fig. 2. The pitch of the grating is constant during the process of oscillation at any a; the deflection from the state of equilibrium is described by equation (3.1). Time averaged fringes can be observed at such amplitudes a_i, $i=1,2,\ldots$ where $E(a_i)=0.5$, or $\frac{2\pi}{\lambda}a_i=r_i$, here r_i denotes i-th root of the 0^{th} order Bessel function of the first kind.

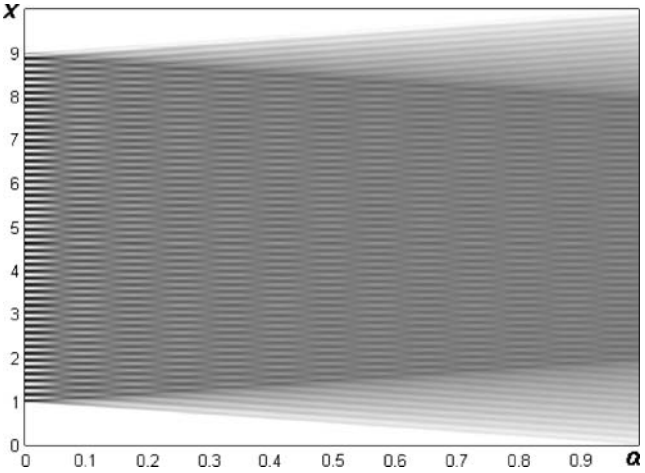

Fig. 2 Time averaged fringes at $u(x, t)=a\ \sin(\omega t+\varphi)$; $\lambda=\pi/20$

Unfortunately, when the deformation is sensitive to coordinate x, for example when $u(x, t)=u(x)\sin(\omega t+\varphi)$,

$$M_5(x)=\lim_{T\to\infty}\frac{1}{T}\int_0^T M_2(x+u(x)\sin(\omega t+\varphi))dt, \tag{3.4}$$

but

$$M_5(x)\neq\frac{1}{2}+\frac{1}{2}\cos\left(\frac{2\pi}{\lambda}x\right)J_0\left(\frac{2\pi}{\lambda}u(x)\right), \tag{3.5}$$

though such relationships as in equation (3.5) can be found even in fundamental papers on time average geometric moiré [5, 6].

As mentioned in the Introduction, the object of this paper is to follow all analytical deductions as strictly as possible in order to derive exact relationships governing the formation of time average moiré fringes. In this paper we will concentrate only on the simplified one-dimensional model comprising of a linear field of oscillating deformations:

$$u(x,t)=ax\sin(\omega t+\varphi). \tag{3.6}$$

Nevertheless, such linear assumption describes a wide class of problems when one end of deformable body is fixed and another end oscillates around its state of equilibrium.

First of all, the instantaneous deformed moiré grating must be expressed in explicit form. Luckily, solution of equation (2.3) is easy when dynamic deflections are described by equation (3.6). $x+ax\ \sin(\omega t+\varphi)=z$ yields $x=\frac{z}{1+a\sin(\omega t+\varphi)}$. Thus, instantaneous deformed grating can be expressed then as:

$$M_2(x,t)=\cos^2\left(\frac{\pi}{\lambda(1+a\sin(\omega t+\varphi))}x\right). \tag{3.7}$$

Then, time averaging yields:

$$\begin{aligned}M_5(x)&=\lim_{T\to\infty}\frac{1}{T}\int_0^T M_2(x,t)dt\\&=\frac{1}{2}\left(1+\frac{1}{2\pi}\int_0^{2\pi}\cos\left(\frac{2\pi x}{\lambda}\cdot\frac{1}{1+a\sin t}\right)dt\right).\end{aligned} \tag{3.8}$$

In other words, one could determine time averaged grayscale intensity if the integral in equation (3.8) could be calculated. Unfortunately, it cannot be expressed in a form comprising ordinary functions.

Calculation of the Special Integral

The considered integral is:

$$I(a,b)=\frac{1}{2\pi}\int_0^{2\pi}\cos\left(\frac{b}{1+a\sin t}\right)dt, \tag{4.1}$$

where $a, b\in\mathbf{R}$, $|a|<1$. The integrand can be expressed in a power series:

$$\cos\left(\frac{b}{1+a\sin t}\right)=\sum_{k=0}^{+\infty}(-1)^k\left(\frac{1}{1+a\sin t}\right)^{2k}\frac{b^{2k}}{(2k)!}. \tag{4.2}$$

Negative whole numbers factorial expansion [19] yields:

$$(1+a\sin t)^{-2k}=\sum_{j=0}^{+\infty}\binom{-2k}{j}a^j(\sin t)^j, \tag{4.3}$$

where the binomial coefficients are expressed like:

$$\binom{-2k}{j}=\frac{(-2k)!}{j!(-2k-j)!}=\frac{(2k+j-1)!(-1)^j}{j!(2k-1)!}. \tag{4.4}$$

It can be noted that at $k=0$ $\binom{0}{0}=1$ and $\binom{0}{j}\equiv 0$ at $j=1,2,\ldots$.

Equation (4.4) holds true, as according to Riordan equality [19], $(-n)!=\pm\infty$; $n=1,2,\ldots$, and $\frac{m!}{n!}=(-1)^{m+n}\frac{(-1-n)!}{(-1-m)!}$; m, $n=0,\pm1,\pm2,\ldots$.

Then, step by step integration yields:

$$I(a,b)=\sum_{j=0}^{+\infty}\sum_{k=0}^{+\infty}(-1)^k\frac{(2k-1+2j)!}{(2j)!(2k-1)!}a^{2j}\frac{(2j-1)!!\ b^{2k}}{(2j)!!\quad(2k)!}$$
$$=\sum_{k=0}^{+\infty}\left((-1)^k\frac{b^{2k}}{(2k)!}\right)+\sum_{j=1}^{+\infty}\sum_{k=1}^{+\infty}\left((-1)^k(2k+2j-1)_{2j}\frac{b^{2k}}{(2k)!}\left(\frac{(a/2)^j}{j!}\right)^2\right)$$
$$=\cos b-b\sum_{j=1}^{+\infty}\sum_{k=0}^{+\infty}\left((-1)^k(2k+2j-1)_{2j-1}\frac{b^{2k+1}}{(2k+1)!}\left(\frac{(a/2)^j}{j!}\right)^2\right), \tag{4.5}$$

where $(m)_n$ is an element of a factorial structure:

$$(m)_0:=1;(m)_1:=m;(m)_n=m(m-1)\cdots(m-n+1);m\in\mathbf{Z}_0;n\in\mathbf{N}. \tag{4.6}$$

Let's introduce the following notation:

$$S_0=\cos b;$$

$$S_j=-b\sum_{k=0}^{+\infty}(-1)^k(2k+2j+1)_{2j-1}\frac{b^{2k+1}}{(2k+1)!},\ j=1,2.... \tag{4.7}$$

Then, the integral can be expressed in the following form:

$$I(a,b)=\sum_{j=0}^{+\infty}\frac{S_j}{(j!)^2}\left(\left(\frac{a}{2}\right)^2\right)^j. \tag{4.8}$$

It is well known [20], that

$$J_0(a)=\lim_{T\to\infty}\frac{1}{T}\int_0^T\exp(ia\sin t)dt$$
$$=\frac{1}{2\pi}\int_0^{2\pi}\cos(a\sin t)dt$$
$$=\sum_{j=0}^{+\infty}\frac{(-1)^j}{(j!)^2}\left(\left(\frac{a}{2}\right)^2\right)^j. \tag{4.9}$$

Thus equation (4.8) can be considered as a generalization of the 0^{th} order Bessel function of the first kind where alternating series $(-1)^j$ is changed by function series S_j.

We will show that S_j can be expressed in the following form:

$$S_j=\sum_{r=0}^{2j-1}b^{r+1}A_{j,r+1}\cos\left(b+r\frac{\pi}{2}\right),\ j=1,2,\ldots, \tag{4.10}$$

where $A_{j,r+1}$ are real constants.

Algorithm for Determination of Constants $A_{j,r+1}$

When j is fixed, the multiplier $(2k+2j+1)_{2j-1}$ in equation (4.7) can be resolved in the following form:

$$(2k+2j+1)_{2j-1}=\sum_{r=0}^{2j-1}A_{j,r+1}(2k+1)_r. \tag{5.1}$$

Equation (5.1) holds true for all $k\in\mathbf{R}$. In order to simplify further transformations we introduce following notations: $p=2k+1$ and $x_r=A_{j,r}$. Then equation (5.1) takes the form:

$$\sum_{r=1}^{2j}(p)_{r-1}x_r=(p+2j)_{2j-1}. \tag{5.2}$$

But $(p)_l=0$ for all $l>p$; $l\in\mathbf{N}$. Equation (5.2) produces a linear system of $2j$ algebraic equations at $p=0,1,2,\ldots,(2j-1)$:

$$\begin{aligned}&x_1=(2j)_{2j-1};\\&x_1+x_2=(1+2j)_{2j-1};\\&\ldots\\&x_1+(2j-1)x_2+\cdots+(2j-1)!x_{2j}=(4j-1)_{2j-1}.\end{aligned} \tag{5.3}$$

System of equations (5.3) can be solved using conventional linear algebra techniques, but the system matrix becomes stiff at higher j. Thus the results produced by non-symbolic solution techniques are contaminated with inevitable rounding errors. Even symbolic solution techniques encounter problems at large j when the system matrix becomes almost singular.

Instead of using standard linear algebra techniques for finding the solution, we will prove that:

$$\begin{aligned}&x_1=(2j)_{2j-1};\\&x_2=(1+2j)_{2j-1}-(2j)_{2j-1};\\&x_3=\tfrac{1}{2}\left((2+2j)_{2j-1}-2(1+2j)_{2j-1}+(2j)_{2j-1}\right);\\&\ldots\\&x_n=\tfrac{1}{(n-1)!}\sum_{l=0}^{n-1}(-1)^l\binom{n-1}{l}(2j+n-1-l)_{2j-1}.\end{aligned} \tag{5.4}$$

Proof First of all we will prove two equalities.

$$\sum_{l=0}^{r}\binom{r}{l}(-1)^l(l)_n=\sum_{l=n}^{r}\frac{r!(-1)^l l!}{(r-l)!l!(l-n)!}=\sum_{l=n}^{r}\frac{r!(-1)^l}{(r-l)!(l-n)!}=\sum_{j=0}^{r-n}\frac{r!(-1)^{j+n}}{j!(r-n-j)!}=$$
$$=\sum_{j=0}^{r-n}\frac{r!(-1)^{j+n}(r-n)!}{(r-n)!j!(r-n-j)!}=(-1)^n(r)_n\sum_{j=0}^{r-n}\binom{r-n}{j}(-1)^j$$
$$=(-1)^n(r)_n(1-1)^{r-n}=0. \tag{5.5}$$

(i) Equation (5.5) is valid for any $n\in\mathbf{N}$.

(ii) The following equality holds true for all $z_k\in\mathbf{R}$:

$$K_r=\frac{(-1)^{r-1}}{(r-1)!}\sum_{k=1}^{l+1}\binom{r-1}{l}(-1)^l(l)_{k-1}z_k$$
$$=\frac{(-1)^{r-1}}{(r-1)!}\sum_{k=1}^{r}\left(\sum_{l=k-1}^{r-1}\binom{r-1}{l}(-1)^l(l)_{k-1}\right)z_k$$
$$=\frac{(-1)^{r-1}}{(r-1)!}\left(\sum_{k=1}^{r-1}\left(\sum_{l=k-1}^{r-1}\binom{r-1}{l}(-1)^l(l)_{k-1}\right)z_k+(-1)^{r-1}(r-1)!z_r\right)$$
$$=z_r+\frac{(-1)^{r-1}}{(r-1)!}\sum_{k=1}^{r-1}\left(\sum_{l=k-1}^{r-1}\binom{r-1}{l}(-1)^l(l)_{k-1}\right)z_k$$
$$=z_r+\frac{(-1)^{r-1}}{(r-1)!}\sum_{k=1}^{r-1}\left(\sum_{l=0}^{r-1}\binom{r-1}{l}(-1)^l(l)_{k-1}\right)z_k=z_r. \tag{5.6}$$

Change of z_k by x_k in equation (5.6) yields $K_r=x_r$. But, equation (5.2) yields:

$$\sum_{r=1}^{l+1}(l)_{k-1}x_k=(l+2j)_{2j-1}. \tag{5.7}$$

On the other hand,

$$K_r=\frac{(-1)^{r-1}}{(r-1)!}\sum_{l=0}^{r-1}(-1)^l\binom{r-1}{l}(l+2j)_{2j-1}$$
$$=\frac{1}{(r-1)!}\sum_{l=0}^{r-1}\binom{r-1}{r-l-1}(-1)^{r-1-l}(l+2j)_{2j-1}. \tag{5.8}$$

Keeping in mind, that $(-1)^l=(-1)^{-l}$ and $r-l-1=n$, equation (5.8) yields:

$$K_r=\frac{1}{(r-1)!}\sum_{n=0}^{r-1}\binom{r-1}{n}(-1)^n(2j+r-n-1)_{2j-1}, \tag{5.9}$$

what results into the determination of x_r, what finally leads to:

$$A_{j,r+1}=\frac{1}{r!}\sum_{l=0}^{r}(-1)^l\binom{r}{l}(2j+r-1)_{2j-1}, \tag{5.10}$$

and that finalizes the proof. □

Some numerical values of coefficients $A_{j,r+1}$ are presented in Table 1.

Example.

$$S_2=-b\sum_{k=0}^{+\infty}(-1)^k(2k+5)_3\frac{b^{2k+1}}{(2k+1)!}$$
$$=\sum_{r=0}^{3}A_{2,r+1}b^{r+1}\cos\left(b+r\frac{\pi}{2}\right)$$
$$=-24b\sum_{k=0}^{+\infty}(-1)^k\frac{b^{2k+1}}{(2k+1)!}-36b^2\sum_{k=0}^{+\infty}(-1)^k\frac{b^{2k}}{(2k)!}$$
$$+12b^3\sum_{k=0}^{+\infty}(-1)^k\frac{b^{2k+1}}{(2k+1)!}$$
$$+b^4\sum_{k=0}^{+\infty}(-1)^k\frac{b^{2k}}{(2k)!}. \tag{5.11}$$

Coefficients $A_{j,r+1}$ grow fast when j and r increase. But the term $(j!)^2$ in the denominator of equation (4.8) grows sufficiently fast. We will show that series in equation (4.8) converges absolutely at all $a,b\in\mathbf{R}$, $|a|<1$. It is clear that

$$\frac{1}{2\pi}\int_0^{2\pi}(1+a\sin t)^{-2k}dt<\frac{1}{2\pi}\int_0^{2\pi}\frac{1}{(1-|a|)^{2k}}dt$$
$$=\frac{1}{\left(1-|a|^{2k}\right)};\ k=0,1,2\ldots. \tag{5.12}$$

Table 1 Coefficients $A_{j,r+1}$

	−1	0	1	2	3	4	5	r
0	1	0	0	0	0	0	0	…
1	0	2	1	0	0	0	0	…
2	0	24	36	12	1	0	0	…
3	0	720	1,800	1,200	300	30	1	…
J	…	…	…	…	…	…	…	$A_{j,r+1}$

On the other hand,

$$\frac{1}{2\pi}\int_0^{2\pi}(1+a\sin t)^{-2k}dt = 1+\sum_{j=1}^{+\infty}\frac{(2k+2j-1)_{2j}}{2^{2j}(j!)^2}a^{2j}. \tag{5.13}$$

Thus,

$$1+\sum_{j=1}^{+\infty}\frac{(2k+2j-1)_{2j}a^{2j}}{2^{2j}(j!)^2} < \frac{1}{(1-|a|)^{2k}}, \tag{5.14}$$

that leads to

$$1+\sum_{k=1}^{+\infty}\left(1+\sum_{j=1}^{+\infty}\frac{(2k+2j-1)_{2j}a^{2j}}{2^{2j}(j!)^2}\right)\frac{b^{2k}}{(2k)!} < 1 + \sum_{k=1}^{+\infty}\frac{1}{(1-|a|)^{2k}}\cdot\frac{b^{2k}}{(2k)!} = \cosh\frac{b}{1-|a|}. \tag{5.15}$$

Thus,

$$|I(a,b)| < \cosh\frac{b}{1-|a|}. \tag{5.16}$$

It can be noted that equation (4.8) is exact (of course when $j=\infty$). In realistic computations j will be always finite, and the result will be an approximation of the integral.

Computational Example

First of all we will observe how the series (4.8) converges to $M_5(x)$ [equation (3.8)] as j increases. It is clear that:

$$M_5(x) = \frac{1}{2}\left(1+I\left(a,\frac{2\pi}{\lambda}x\right)\right), \tag{6.1}$$

where $I(a, b)$ is defined by equation (4.1) and $M_5(x)$ is defined by equation (3.4).

$M_5(x)$ can be also approximated using computational techniques:

$$M_5(x) = \frac{1}{2}\left(1+\lim_{k\to\infty}\frac{1}{k}\sum_{j=1}^{k}\cos\left(\frac{2\pi x}{\lambda}\left(a\sin\left(\frac{2\pi}{k}j\right)\right)^{-1}\right)\right). \tag{6.2}$$

$M_5(x)$ is shown in Fig. 3 (at a=0.1 and $\lambda=\pi/20$); here solid line stands for the approximation based on the limit sum [at k=1,000 in equation (6.2)]; dashed lines stand for approximations based on equation (4.8) at j=1, j=5 and j=10 accordingly. First two fringes can be clearly seen at around x=0.6 and x=1.35.

Next, we will demonstrate the difference between the pattern of time averaged fringes produced by equation (3.2) and equation (3.4). We assume linear field of oscillating deformations [as defined in equation (3.6)] and construct one-dimensional time averaged image (M5(x) in Fig. 4) at a=0.05; $\lambda=\pi/20$ and L=9, where L is the length of one-

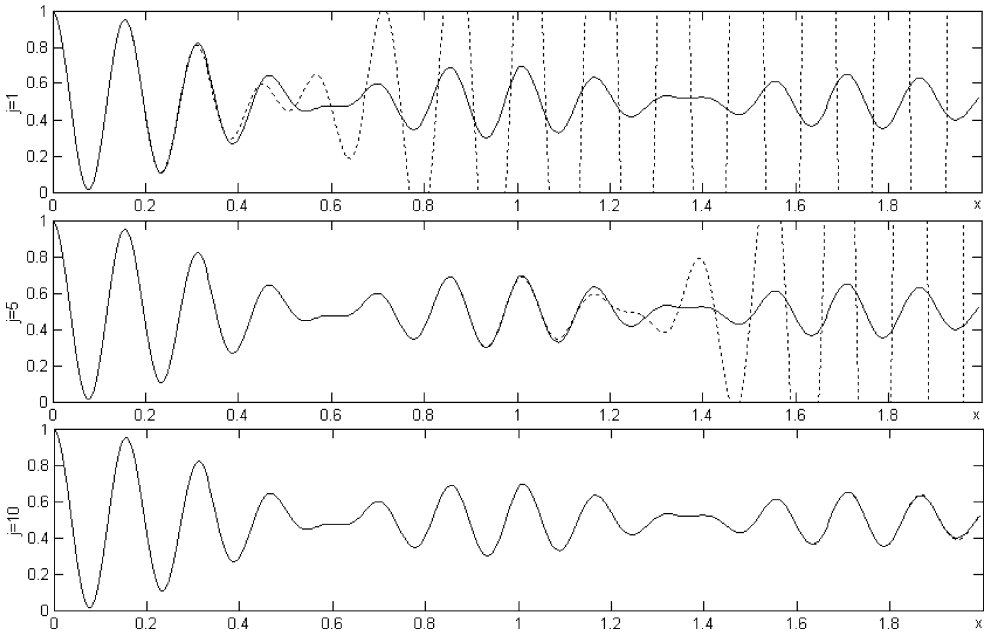

Fig. 3 Approximations of $M_5(x)$ at a=0.1 and $\lambda=\pi/20$

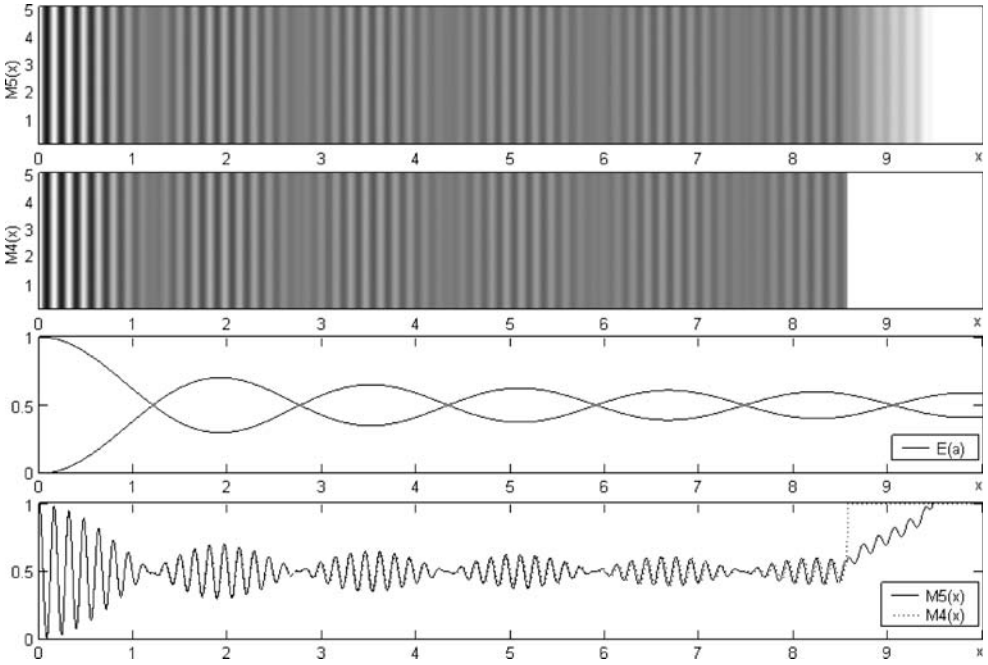

Fig. 4 Comparisons between $M_5(x)$ and $M_4(x)$ at $\lambda=\pi/20$; $a=0.05$ and $L=9$

dimensional structure in the state of equilibrium (the background is white). We visualize an optical equivalent of the one-dimensional function (0 value corresponds to black color; 1—to white color) instead of plotting a line graph. The left part of the structure is motionless; sharp moiré grating lines can be seen there. The right side of the structure experiences maximum cyclic deformation, and the amplitude there is equal to $aL=0.45$.

Analogously, we construct a one-dimensional optical image described by equation (3.5) (M4(x) in Fig. 4) in the region $0\le x\le L(1-a)$. It is hard to notice any considerable differences between those two images, therefore we visualize the envelope function of $M_4(x)$ (determined by equation (3.3) and labeled as E(a) in Fig. 4). Also, one-dimensional line graphs of $M_5(x)$ (solid line) and $M_4(x)$ (dotted line) are plotted in the last section of Fig. 4(a). One can notice small differences between these two lines at the right side of the drawing.

The differences between $M_5(x)$ and $M_4(x)$ are much more apparent at a higher amplitude a (Fig. 5) where the length of the structure in the state of equilibrium is $L=7$ and the amplitude at the right end is $aL=2.1$.

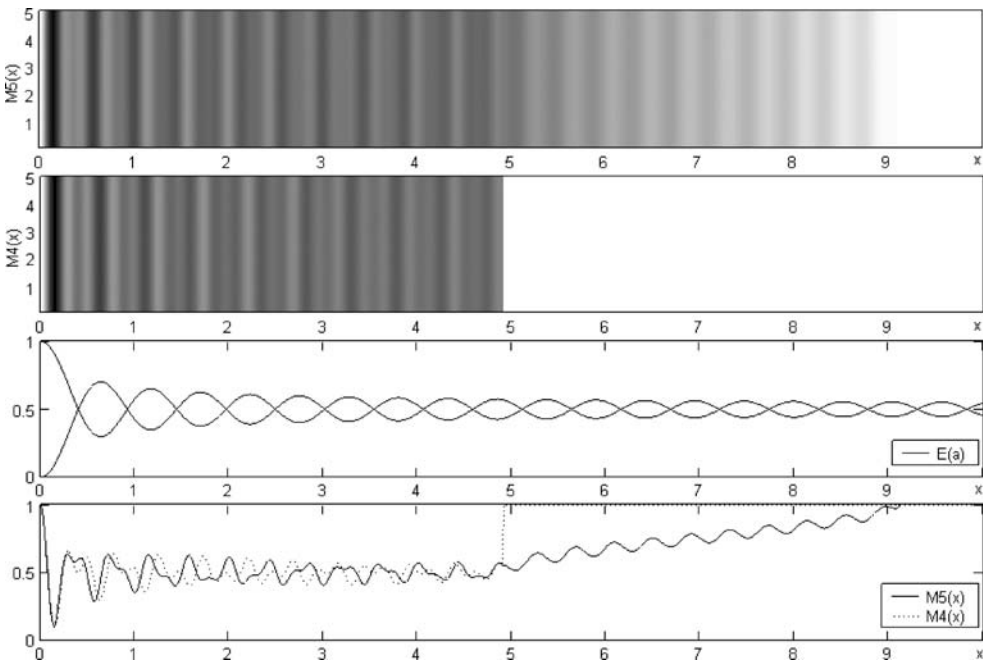

Fig. 5 Comparisons between $M_5(x)$ and $M_4(x)$ at $\lambda=\pi/10$; $a=0.3$ and $L=7$

Inverse Problem of Fringe Interpretation

In general, interpretation of experimental results produced by optical fringe-based whole-field non-destructive analysis techniques comprises two basic steps. The first one is the enumeration of fringes. This can be performed manually or exploiting automatic or semi-automatic fringe counting techniques [4]. The second step is an inverse problem which is solvable if and only a relationship between the fringe number and the magnitude of the measured physical quantity is known. Theoretical foundation of all fringe-based experimental techniques is based on the fact that fringe centre lines serve as isolines of the measured quantity. Then computational routines can be exploited for numerical reconstruction of three-dimensional maps of that quantity.

We will show that fringes produced by time average moiré, in general, do not represent a pattern of isolines of amplitude if only dynamic deformations are assumed. This fact is rather surprising as time average geometric moiré is considered a well-established optical experimental technique with numerous practical applications.

First of all we construct a time averaged image similar to the image constructed in Fig. 2. The difference now is that we consider dynamic deformations described by equation (3.6). Amplitude of oscillation varies along horizontal y-axis in Fig. 6. The length of one-dimensional system in the state of equilibrium is equal to 5 (for all y). The amplitude of oscillation of any point around the state of equilibrium (in the area $0\le x\le 5$; $0\le y<1$) is determined by the following relationship:

$$a(x,y)=\frac{1}{5}xy. \tag{7.1}$$

The amplitude is zero at $y=0$, and one can see the moiré grating clearly at the left side of Fig. 6. At larger y the grating lines become blurred due to time averaging and overlap with moiré fringes. At $y=1$ the one-dimensional system is compressed into a point and extended up to the double equilibrium length for every period of oscillation.

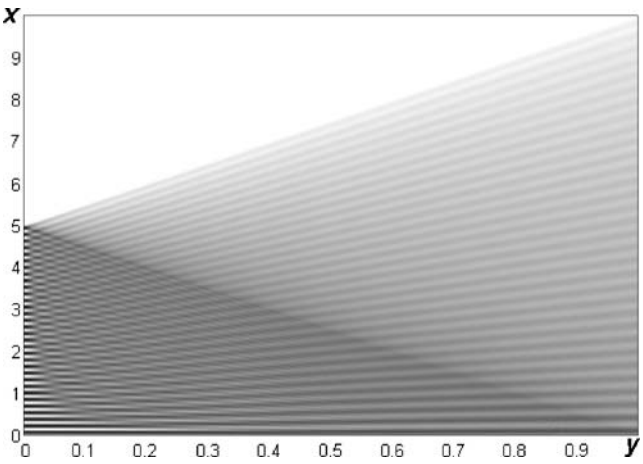

Fig. 6 Time averaged image at $L=5$; $\lambda=\pi/20$; $a=y$

The shape of time averaged moiré fringes in Fig. 6 appears to be hyperbolic. If the formation of time averaged moiré fringes would be governed by equation (3.2), then the fringes would be shaped as hyperbolas. It follows from equation (3.3) that the centerlines of the fringes must be located at such points where the amplitude is such that the argument of the 0^{th} order Bessel function coincides with its root. In other words, the equation for the i-th time averaged fringe can be deduced from the equality

$$\frac{2\pi}{\lambda}a(x,y)=r_i, \tag{7.2}$$

where r_i is the i-th root of 0^{th} order Bessel function of the first kind. Equation (7.1) yields:

$$x=\frac{5r_i\lambda}{2\pi y}. \tag{7.3}$$

We will show that the centerlines of time averaged fringes in Fig. 6 are not hyperbolas. We will use moiré gratings with variable pitch for that purpose. We will select such relationship between λ and y that hyperbolas in Fig. 6 would be mapped into an array of straight horizontal lines.

Let's assume that points (y_1, x_1) and (y_2, x_2) belong to the i-th hyperbola. Then, from equation (7.3) it follows that $x_k=\frac{5r_i\lambda}{2\pi y_k}$; $k=1,2$. We fix λ at y_1 but change the pitch at y_2 in such a way that x_2 should be equal to x_1:

$$\widetilde{\lambda}=\frac{y_2}{y_1}\lambda, \tag{7.4}$$

where $\widetilde{\lambda}$ is the pitch at y_2.

The transformed static moiré grating (at fixed $y_1=0.05$) is shown in Fig. 7. It is clear that $\lim_{y_2\to 0}\widetilde{\lambda}=0$. Aliasing effects can be seen in the left side of Fig. 7. These effects are due to the limited number of sampling points (pixels) used to visualize moiré gratings with extremely small pitch.

As mentioned previously, such a grating with variable pitch would map a pattern of time averaged fringes (if only their centerlines are hyperbolas) into an array of parallel horizontal fringes. We will illustrate this effect assuming that the formation of time averaged fringes is governed by equation (3.2):

$$M_4\left(x,y,\widetilde{\lambda}\right)=\frac{1}{2}+\frac{1}{2}\cos\left(\frac{2\pi}{\widetilde{\lambda}}x\right)J_0\left(\frac{2\pi}{5\widetilde{\lambda}}xy\right). \tag{7.5}$$

Numerically produced fictitious pattern of time averaged fringes is presented in Fig. 8(a). Grayscale intensity at the centerlines of the fringes is equal to 0.5; digital contrast enhancement techniques [21] help to highlight the fringes [Fig. 8(b)].

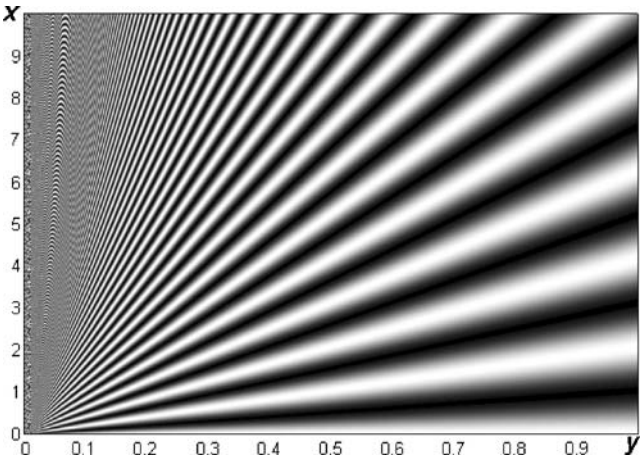

Fig. 7 Static moiré grating with variable pitch at $y_1=0.05$

Figure 8(b) is a clear illustration that if the formation of time averaged fringes would be governed by equation (3.2), time average geometric moiré could be considered as a classical optical experimental technique because time averaged fringes would represent isolines of amplitudes. Unfortunately, the situation is different as the formation of time averaged fringes is governed by equation (3.8) instead. The mapped pattern of time averaged fringes is shown in Fig. 9(a); filtered and highlighted fringes—in Fig. 9(b).

It can be seen that time averaged fringes do not form an array of parallel horizontal lines in Fig. 9(a). One should not be confused by thick black fringes at the right side of Fig. 9(a). It can be seen that the density of those fringes in Fig. 7 is almost double compared to Fig. 9(a). Actually, the same effect is observed in Fig. 6 where the density of time-averaged fringes at the right boundary is almost double compared to the density of grating lines at the left boundary. This effect can be explained exploiting terminology sometimes used by optical engineers whenever time averaging techniques are applied for harmonic oscillations [22]: oscillating structure "stays for the longest periods of time at the positions of extreme deflections from the state of equilibrium". Of course, exact formation of time average

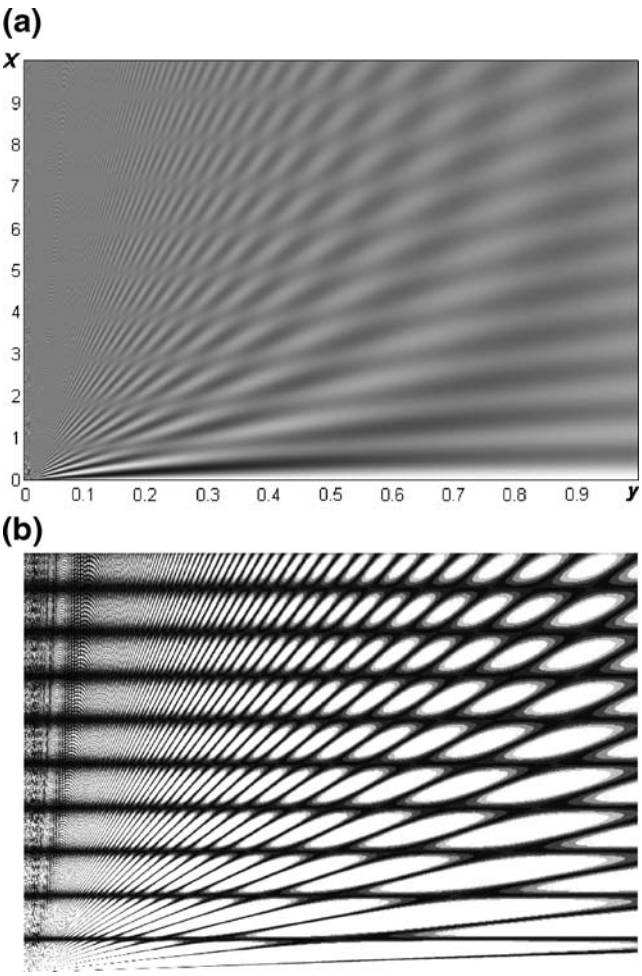

Fig. 8 Fictitious pattern of time averaged fringes: (**a**) image without filtering; (**b**) filtered digital image

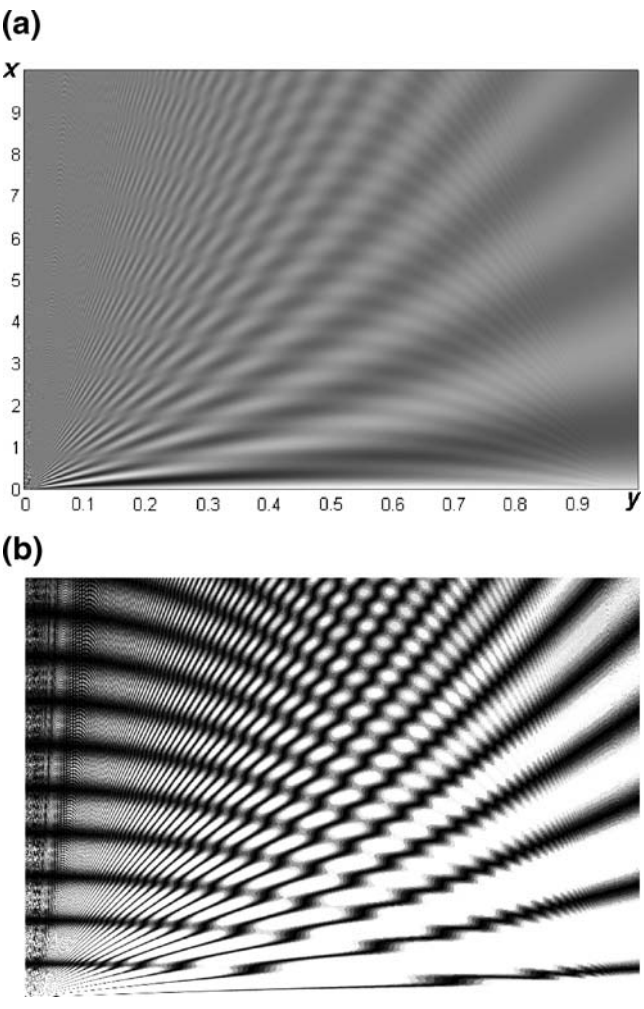

Fig. 9 Pattern of time averaged fringes generated by moiré grating with variable pitch: (**a**) image without filtering; (**b**) filtered digital image

geometric moiré fringes is governed by equation (3.8), but such an engineering approach can explain the beforementioned effect. At $a=1$ elastic one-dimensional system is compressed into a point and extended up to its double length in every period of harmonic oscillations. No instantaneous fringes are generated when the system is compressed into a point. But instantaneous pitch at the moment when the system is doubly extended is double compared to the pitch in the state of equilibrium. This effect can be observed both in Figs. 6 and 9(a).

The density of fringes at the right boundary in Fig. 9(b) is again double compared to Fig. 9(a), but that is due to the application of contrast enhancement technique which maps middle grayscale levels to black and all other grayscale levels to white. Therefore every dark fringe in Fig. 9(a) is represented by two dark fringes in Fig. 9(b). Usually such parasitic fringes are wiped out from the digital image by the help of pixel based morphological operations [21], but we did not apply these techniques because the thickness of constitutive grating lines is variable in our computational set-up.

Time averaged moiré fringes can be clearly observed at the left part of the digital image in Fig. 9(b). The fact that these fringes are not horizontal has only one meaning—the relationship between the fringe order and the amplitude of oscillation is implicit and depends from the amplitude itself. In other words, in order to know what is the amplitude of oscillation at the centerline of the i-th fringe, one must know the magnitude of that amplitude in advance. That betrays the fundamental principle of optical whole field fringe based experimental techniques—pattern of fringes produced by time averaged geometric moiré cannot be used for identification of the magnitude of the measured quantity. That is a rather astonishing and depressing fact keeping in mind that time average geometric moiré is considered as a classical and well established experimental method.

Anyway, the amplitude of oscillations in realistic physical experiments usually is comparatively small. Elastic objects are rarely compressed to a half of their length in a period of oscillation (what corresponds to $a=0.5$). The pattern of fringes in Figs. 8(b) and 9(b) almost coincide in the region where the relative amplitude of oscillations it not larger than 0.1. Therefore equation (7.2) can be used for approximate estimation of amplitudes in this region. Of course, one must have in mind that the inverse problem gets much more complicated when the amplitude of oscillation becomes higher.

Concluding Remarks

Time average geometric moiré is a classical optical experimental technique exploited in different engineering applications. Surprisingly, the theoretical basis of the inverse problem for this technique was based on the assumption that either the pitch of the moiré grating does not vary in time, or this variation is very slow.

We tried to focus our attention on the derivation of the relationships governing the formation of time averaged fringes as strictly as possible. Produced results were rather unexpected. Classical relationship between the fringe order and the amplitude of oscillation holds true when non deformable bodies oscillate around the state of equilibrium. But this relationship becomes implicit when a deformable body is considered. In such situations in-plane time average geometric moiré is applicable only for small oscillations.

References

1. Shang H, Xie H, Wang X, Jiang S, Dai F, Wang W et al (2005) Thermal properties measurement of micro-electromechanical system sensors by digital moiré method. Strain 41:157–162. doi:10.1111/j.1475-1305.2005.00226.x.
2. Han A (1998) Recent advancements of moiré and microscopic moiré interferometry for thermal deformation analyses of microelectronics devices. Exp Mech 38:278–288.
3. Sciammarella CA, Sciammarella FM, Kim T (2003) Strain measurements in the nanometer range in a particulate composite using computer-aided moiré. Exp Mech 43:341–347. doi:10.1007/BF02410533.
4. Kobayashi AS (1993) Handbook on experimental mechanics, 2nd edn. SEM, Bethel.
5. Patorski K, Kujawinska M (1993) Handbook of the moiré fringe technique. Elsevier, Oxford.
6. Field JE, Walley SM, Proud WG, Goldrein HT, Siviour CR (2004) Review of experimental techniques for high rate deformation and shock studies. Int J Impact Eng 30:725–775. doi:10.1016/j.ijimpeng.2004.03.005.
7. Post D, Han B, Ifju P (1997) High sensitivity moiré: experimental analysis for mechanics and materials. Springer, Berlin.
8. Dai FL, Wang ZY (1999) Geometric micron moiré. Opt Lasers Eng 31:191–198. doi:10.1016/S0143-8166(99)00020-2.
9. Liang CY, Hung YY, Durelli AJ, Hovanesian JD (1979) Time-averaged moiré method for in-plane vibration analysis. J Sound Vib 62:267–275. doi:10.1016/0022-460X(79)90026-9.
10. Lin CJ, Chiang FP (1982) Time-average in-plane moiré method for the analysis of nonsinusoidal cyclic loading. Exp Mech 22:64–68. doi:10.1007/BF02326078.
11. Mitchell AK (2005) Optical modal analysis using white-light projected fringes. Exp Mech 45:250–258. doi:10.1007/BF02427949.
12. Asundi A (1994) Novel techniques in reflection moiré. Exp Mech 34:230–242. doi:10.1007/BF02319760.
13. Ragulskis M, Maskeliunas R, Ragulskis L, Turla V (2005) Investigation of dynamic displacements of lithographic rubber roller by time average geometric moiré. Opt Lasers Eng 43:951–962. doi:10.1016/j.optlaseng.2004.10.004.
14. Sciammarella CA (2003) Overview of optical techniques that measure displacements: Murray lecture. Exp Mech 43:1–19. doi:10.1007/BF02410478.
15. Munoz-Rodriguez JA, Rodriguez-Vera R (2004) Image encryption based on moiré pattern performed by computational algorithms. Opt Commun 236:295–301. doi:10.1016/j.optcom.2004.03.089.
16. Sciammarella CA (1965) Basic optical law in the interpretation of moiré patterns applied to the analysis of strains—part 1. Exp Mech 5:154–160. doi:10.1007/BF02324049.

17. Voloshin AS, Burger CP, Rowlands RE, Richard TG (1986) Fractional moiré strain analysis using digital imaging techniques. Exp Mech 26:254–258. doi:10.1007/BF02320050.
18. Ning PT, Peng WL (1988) Automatic analysis of moiré fringe patterns by using an image-processing system. Exp Mech 28:350–354. doi:10.1007/BF02325175.
19. Riordan J (1968) Combinatorial identities. Wiley, New York.
20. Watson GN (1995) A treatise on the theory of Bessel functions. Cambridge University Press, Cambridge.
21. Ragulskis M, Saunoriene L (2006) Applicability of optical geometric differentiation for time average geometric moiré. Strain 42:173–179. doi:10.1111/j.1475-1305.2006.00273.x.
22. Vest CM (1979) Holographic interferometry. Wiley, Ontario.